UNIZIK JOURNAL OF ENGINEERING AND APPLIED SCIENCES (UJEAS)

Research Article

Multi-Input Single Output (MISO) modelling with Adaptive Neuro Fuzzy Inference System (ANFIS) and Response Surface Methodology (RSM) for adsorptive removal of Erythrosine B dye from wastewater using activated carbon derived from agrowaste

Okoye, C. C., Onukwuli, O. D., Okey-Onyesolu, C. F., Onu, C. E.

Special Issue
A Themed Issue in Honour of Professor Onukwuli Okechukwu Dominic (FAS).

This special issue is dedicated to Professor Onukwuli Okechukwu Dominic (FAS), marking his retirement and celebrating a remarkable career. His legacy of exemplary scholarship, mentorship, and commitment to advancing knowledge is commemorated in this collection of works.

Edited by
Chinonso Hubert Achebe PhD.
Christian Emeka Okafor PhD.

UJEAS

UNIZIK JOURNAL OF ENGINEERING AND APPLIED SCIENCES

UNIZIK Journal of Engineering and Applied Sciences 4(1), March (2025), 1784 - 1801
Journal homepage: https://journals.unizik.edu.ng/index.php/ujeas
PRINT ISSN: 2992-4383 || ONLINE ISSN: 2992-4391

Multi-Input Single Output (MISO) modelling with Adaptive Neuro Fuzzy Inference System (ANFIS) and Response Surface Methodology (RSM) for adsorptive removal of Erythrosine B dye from wastewater using activated carbon derived from agrowaste

Okoye, C. C.[*1], Onukwuli, O. D.[1], Okey-Onyesolu, C. F. [*1], Onu, C. E. [1]

[1]Department of Chemical Engineering, Nnamdi Azikiwe University, PMB 5025, Awka, Anambra State
[*]CorrespondingAuthor's E-mail:cc.okoye@unizik.edu.ng, cf.okey-onyesolu@unizik.edu.ng

Abstract
The adaptive neuro-fuzzy inference system (ANFIS) and response surface methodology (RSM) were employed to model erythrosine B (EB) dye adsorptive uptake from wastewater using acid and thermal activated tamarind seeds (Dialium guineese) as adsorbent. Fourier Infrared Spectroscopy and Scanning Electron Microscopy were used to identify the functional groups and surface morphology of the tamarind seed activated carbon (TSAAC) respectively. The adsorption kinetics of EB dye uptake on TSAAC was described by the pseudo-first order (PFO), pseudo-second order (PSO), Elovich and Intra-particle diffusion models. Analysis of Variance was employed to determine if there is a statistical significance difference between the percentages of EB dye adsorbed on TSAAC at various time intervals and Tukey's HSD post hoc analysis to spot where these differences occurred. RSM and ANFIS models were evaluated using the coefficient of determination (R^2), Marquadt's Percent Standard Deviation (MPSD), The hybrid fractional error function (HYBRID) and Average Relative Error (ARE) metrics. Results revealed that the PSO model best fitted the kinetics experimental data when compared with the Elovich and PFO models. Intra-particle diffusion plots showed that there are other rate-limiting steps that control the adsorptive process besides intra-particle diffusion. ANOVA results established statistically significant difference between the percentages of EB dye adsorbed on TSAAC at various time intervals. Both RSM and ANFIS recorded high coefficient values of 0.999 and 0.998 indicating strong predictive capability in predicting the adsorption of EB dye. Further statistical investigations revealed that ANFIS outperformed RSM in approximating the nonlinear behaviour of the adsorptive system. An optimum adsorption efficiency of 96.73% was achieved using genetic algorithm. This study has successfully revealed the capability of both RSM and ANFIS in modeling the adsorptive removal of EB dye using TSAAC.

Keywords: Adsorption, ANFIS, RSM, tamarind seeds, kinetics, genetic algorithm

1. Introduction

Since water is the primary nutrient for all living things, it is necessary for all industrial, metabolic, and environmental processes (Yaqub et al., 2023). Worldwide, the issue of different pollutants contaminating water is becoming more prevalent (Akpomie and Conradie, 2020). These days, unchecked rapid industrialization, agricultural expansion, and the abrupt global population boom are all contributing to the alarming rise in freshwater consumption (Nure et al., 2023). By 2030, everyone should have access to safe, reasonably priced, clean, and enough water, according to Sustainable Development Goal 6 (Nure et al., 2023; Wang et al., 2022). Dye pollution of aquatic ecosystems is one of the obstacles to reaching this ambitious goal. Among metal ions, dyes, insecticide sprays, and other pollutants, dye pollution is the one that harms the environment the most. The presence of stable aromatic rings makes dyes poisonous and non-biodegradable. (Alardhi et at., 2023). Indiscriminate discharge of

untreated dye wastewater effluent into our aquatic bodies such as streams, lakes and rivers is a major cause of water scarcity and quality deterioration. By 2030, 40% of the world's population is predicted to experience lack of water, which is essentially defined as freshwater availability below 1000 L per person annually. (Nure et al., 2023).

One significant contributor to aesthetic pollution, eutrophication, and disturbances to aquatic life is the introduction of colored wastewater into the ecosystem (Fito et al., 2023). Because of their toxicity and detrimental effects on photosynthetic activity, synthetic dyes are a group of contaminants that wastewater must be cleaned of before being released into aquatic environments (Serban et al., 2023; Tomar et al., 2023). Since light absorption decreases algal photosynthetic behavior and has a major impact on food chains, the primary environmental concern of coloring is the absorption and reflection of sunlight entering water bodies. (Serban et al., 2023; Garcia et al., 2023; Yaqub et al, 2023). Azo dyes are a broad class of synthetic dyes that contain azo groups (–N=N–) among the various organic dyes, which can be anionic, cationic, or nonionic. Azo dyes are extremely toxic, carcinogenic, and teratogenic due to their aromatic rings and -N=N- groups, which also make them detrimental to the environment and living things (Hambisa et al., 2023). Water-soluble anionic xanthene dyes, of which erythrosine B is a member, are widely used, particularly in the cosmetic, food and pharmaceutical sectors. (Pipíška et al., 2022).

A common xanthene coloring agent, erythrosine B (EB) is extremely toxic to people and can result in a number of negative health outcomes, such as cancer and different kinds of allergies (Elfadil et al., 2022). Because of their high water solubility, EB is infamously resistant to traditional wastewater treatment methods, such as biological activated sludge (Nascimento et al., 2022). Many environmental studies focus on dyes because of their possible toxicity and carcinogenicity, with the goal of removing them from wastewater through adsorption processes. (Pipíška et al., 2022)

The chemical, physical and biological techniques utilized to remove dye from wastewater include filtration, coagulation, advanced oxidation, ion exchange, bioremediation, activated sludge mechanisms, and precipitation (Zayed et al., 2023). On the other hand, these technologies are not sustainable and demand a significant financial outlay. In contrast to those technologies, adsorption technology has been applied to wastewater remediation in numerous significant industrial applications. Adsorption is inexpensive, simple to use, and safe for the environment and the economy. (Fito and others, 2023).Furthermore, the adsorption method has benefits like a reusable and easily accessible adsorbent. Zeolite, biomaterials, activated carbon, fly ash, nanoparticles, biomass, and polymers are examples of commonly used adsorbent materials. (Hung et al., 2023).

Because it is an inexpensive natural material and has a large surface area, activated carbon is unique among these materials and has a good adsorption capacity for anionic dyes. However, there are certain restrictions on the activated carbon's regeneration following adsorption, which raises the cost of the treatment procedure (Phothitontimongkol and Prasertboonya, 2024). Agricultural waste-derived biomass has drawn special attention as a desirable substitute for adsorbents due to its high reactivity and chemical stability, which are caused by repeating functional groups in the cellulosic chain. (Abisha et al., 2022). The agricultural wastes such as rice husk, waste from ginger, soya oil extract, peelings of lemon, cane sawdust, tamarind shells, maize, powder of seashells, and papaya fruit seeds are low-cost adsorbents (Sulthana et al., 2022). Tamarind seeds (*Dialium guineese*) was used in this study. It is abundant in the rain forest region of West Africa. It is sparingly used. To enhance its usage, tamarind seeds were considered a precursor for activated carbon production in this study.

This research studied the adsorptive removal efficiency of EB dye as a representative molecule of a anionic dye by utilizing the activated carbon gotten from frequently unused tamarind seeds. Pseudo First Order (PFO), Pseudo Second Order (PSO) and Elovich models were employed to understand the kinetic mechanisms of the uptake of EB dye on activated carbon derived tamarind seeds. ANOVA statistical tools was used to investigate if there is a statistical significant difference between the adsorptive removal efficiency of derived activated carbon at different predetermined time intervals using the Tukey's Honest Significant Difference test. In contrast to the traditional one-factor at a time (OFAT), Response Surface Methodology (RSM) and the Adaptive Neuro-fuzzy Inference System (ANFIS) were thought to be more reliable tools for modeling the behavior of the adsorptive process. Despite being straightforward and simple to use, OFAT, an experimental design that varies one parameter while holding all other parameters constant, may not be effective in system that deals with dye ions uptake because the factors influencing dye removal are usually nonlinear and interdependent. As a result, OFAT might not be able to determine the ideal circumstances for a system or process and might overlook important interactions between the variables. (Banza et al.,2023). This research therefore, integrated experimental data set in an expert system, ANFIS, to predict the

adsorptive capability of tamarind seed derived activated carbon in remediating EB dye wastewater hence the novelty of this work.

2.0 Materials and methods

Tamarind Seeds (TS) – *Dialium guineense* used in this research was obtained from Amasiri in Ebonyi state, Nigeria. The seeds were washed very well with water at least for four times to remove all unwanted materials, dirt, sand, etc. The already washed tamarind seeds were air dried, then dried in the oven at temperature of 110^{o}C. The raw materials were carbonized in a muffle furnace for 1 hour at 600^{0}C. The sample that had been carbonized was soaked in a 60% by weight phosphoric acid (H_3PO_4) at a ratio of 1:1 wt basis of activating agent to tamarind seed. After being vigorously stirred, the slurry was left for a full day. De-ionized water was used to wash the resulting carbons until the pH of the leachate was between 6 and 8, then dried for five to six hours at 105˚C in an oven. The activated carbon dried in the oven carbon was size-reduced with mortar and pistil, sieved through a 75µm mesh screen. The produced tamarind seed acid activated carbons (TSAAC) were kept in airtight containers with the appropriate labels. One gram of EB dye was dissolved in one liter of de-ionized water to get ready a 1000 mg/l stock solution. The stock solution was serially diluted to prepare other dye concentrations.

2.1 Characterization

The Shimadzu FTIR 8400 FTIR spectrophotometer and PhonemProx scanning electron microscope were utilized to characterize the sample. The activated carbon's functional groups were identified using the results of FTIR spectra. The SEM micrograph showed the activated carbon's morphology.

2.2 Adsorption tests

The dye ions uptake rate by the adsorbents was investigated at different temperature range (30, 40 and 50^{o}C). At constant pH, 1g of adsorbent and 100ml of the solvent, a batch-wise experiment was carried out. At defined times about 10ml of the solution were taken. After filtering the withdrawn solution, the supernatant solution's concentration was determined and recorded. PFO, PSO, Elovich and Interparticle diffusion kinetic models were investigated to depict the rate of dye ions uptake. Below are equations (1) and (2) for the calculation of the % dye adsorbed and sorption capacity,

$$\% \text{ Adsorbed} = \frac{(Co-Ce)}{Co} x \frac{100}{1} \quad (1)$$

$$qe = \frac{(Co-Ce)V}{m} \quad (2)$$

m, q_e, C_e and C_o is the weight of adsorbent (g), amount of dye adsorbed (mg/g), concentration of dye (mg/L) at time t and initial time, respectively.

2.3 Adsorption Kinetics

The rate-limiting steps and the adsorption rate can be evaluated by the adsorption kinetics study. Understanding the adsorption rate is crucial for assessing an adsorbent's performance. Furthermore, an adsorbent's performance can be enhanced by comprehending the rate-limiting step. For instance, increasing the adsorbent's porosity can hasten the adsorption process if internal diffusion is the rate-limiting step (Wang and Guo, 2023). This study tested the suitability of PFO, PSO, Elovich and Intra-particle diffusion kinetic models (Table 1) in describing the kinetic experimental data gotten from the uptake of EB dye onto TSAAC.

Table 1: Kinetic Models

S/N	Model	Equation	Eqn no	Ref
1	Pseudo First Order	$\ln(q_e - q_t) = \ln q_e - k_1 t$	3	Surela et al. (2024)
2	Pseudo-Second Order	$\frac{t}{qt} = \frac{1}{k2qe2} + \frac{t}{qe}$	4	Revellame et al. (2020)
3	Elovich	$q_t = \frac{1}{\beta}\ln(\alpha\beta) + \frac{1}{\beta}\ln t$	5	Surela et al. (2024)
4	Intra-particle	$q_t = ki_d t^{1/2} + I$	6	Benjelloun et al. (2021)

where qt: amount of adsorbate in the adsorbent at time t (mg g^{-1}); q_e denotes the amount adsorbed at equilibrium, (mgg^{-1}), k_1 (min^{-1}) is the PFO adsorption kinetic parameter, k_2 (g mg^{-1} min^{-1}) is the PSO adsorption kinetic parameter; α and β are the initial adsorption rate (mg g^{-1} min) and the extent of surface coverage and the activation energy for chemisorptions (g mg^{-1}); I is the intercept which represents the thickness of the boundary layer. Thicker boundary layer is characterized by larger intercept, intra-particle diffusion rate constant is represented by ki_d ($mg/gmin^{-1/2}$).

2.4 Statistical comparative analysis

2.4.1 Analysis of variance (ANOVA)

ANOVA was used to compare the independent groups' means.

2.4.2 Tukey's honest significant difference (HSD) test

A new critical value that can be used to determine if there are significant differences between any two sets of means was established by Tukey's test. Because it deals with the mean difference that must be surpassed in order to attain significance, the crucial value is somewhat different. Therefore, one just computes a single critical value and then the difference between every pair of alternative means. The Tukey critical value is then compared to each difference. The comparison is significant if the difference exceeds the Tukey value (Okoye et al., 2019).

2.5 Design of Experiment

The Central Composite Design technique of the Response surface methodology was used to generate a matrix to model the adsorption of EB dye ions on TSAA using the Design Expert software trial version 10. In order to generate a model and to investigate the combined effects of the four independent variables (factors) namely: adsorbent dosage, contact time, solution temperature and pH, a set of thirty experiments were performed. Preliminary experiments were used to determine the low and high levels of adsorption effective variables. Adsorbent dosage of 2.0 and 4.0g, contact time of 60 and 120mins, temperature of 40 and 60°C and pH of 4 and 8 were the software's inputs for the marginal conditions of the effective variables. Table 2 displays the factor levels and their corresponding real values.

Table 2: Experimental range of the independent variables

Independent variable	**Symbol**	**Range and Levels**				
		-α	**-1**	**0**	**+1**	**+α**
Dosage (g)	A	1	2	3	4	5
Contact time (mins)	B	30	60	90	120	150
Temperature (^{0}C)	C	30	40	50	60	70
pH	D	2	4	6	8	10

2.6 ANFIS

The EB dye adsorptive removal efficiency of TSAAC was modelled using the RSM experimental dataset with pH, temperature, time and adsorbent dosage as inputs and % EB dye adsorbed as output. The triangular membership function (trimf) and linear membership function were used for the input and output variables respectively. The number of membership functions for each input was set at two. The IF-THEN rule-based Sugeno inference method served as the foundation for the ANFIS model. The ANFIS model structure is presented in Figure 1. The input parameters and output variables are represented by the first and last layers of the ANFIS structure.

2.7 **Model Performance Indices**

The potential of the RSM and ANFIS models to capture the behaviour of the response variable (% EB dye adsorbed) was evaluated by coefficient of determination (R^2), Marquadt's Percent Standard Deviation (MPSD), The hybrid fractional error function (HYBRID) and Average Relative Error (ARE):

$$MPSD = 100\sqrt{\frac{1}{n-p}\sum_{i=1}^{n}\left(\frac{y_i - \bar{y}_i}{y_i}\right)^2} \quad (7)$$

$$HYBRID = \frac{100}{n-p}\sum_{i=1}^{n}\left(\frac{y_i - \bar{y}_i}{y_i}\right)^2 \quad (8)$$

$$ARE = \frac{1}{n}\sum_{i=1}^{n}\left|\frac{y_i - \bar{y}_i}{y_i}\right| \quad (9)$$

Where n = total number of observations; p = total number of model parameters; $\bar{y}_i$= calculated or predicted value of yi; y_i = experimental response for ith observation; (Revellame et al., 2020). The values calculated for MPSD, HYBRID and ARE, are indirectly proportional to the goodness of fit.

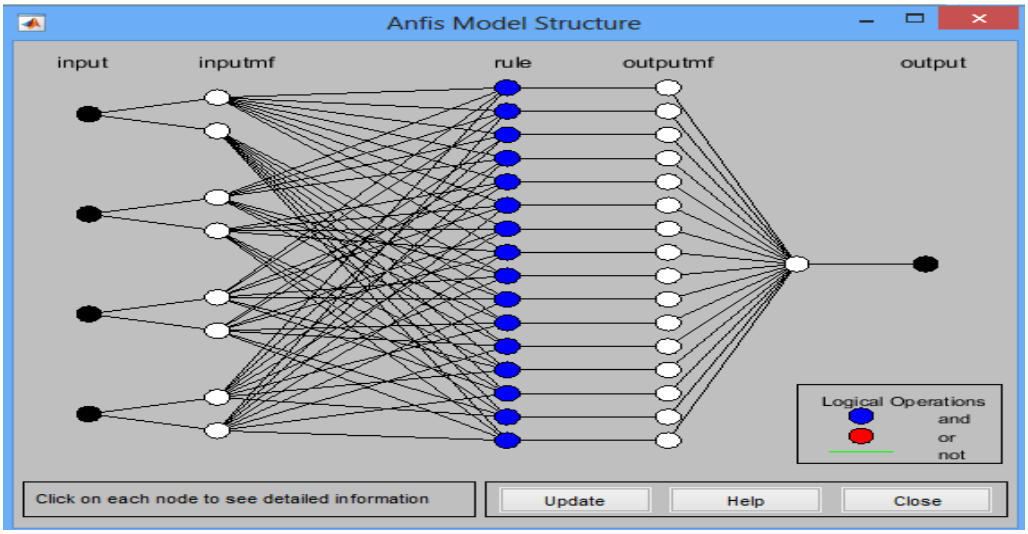


Figure 1:Anfis Model Structure

3.0 Result and Discussion

3.1 Adsorbent Characterization

Fig. 2 depicts a plot of %Transmittance against wave numbers for TSAAC. From the spectrum, peak 3896cm^{-1} indicates the existence of O-H stretch, free hydroxyl, phenol, 3780cm^{-1}, O-H stretch, free hydroxyl, alcohols. The band observed at 3396cm^{-1} and 3251cm^{-1} are attributed to hydroxyl group, H-Bonded OH stretch respectively. The bands at 2935, 1641, 1506 cm^{-1} represent asymmetric C-H stretch, alkenyl C=C stretch and aromatic nitro compounds. Additional bands found can be attributed to C-C stretch (in-ring), aromatic C-H in plane bend and alcohol, OH out-of-plane bend (Coates, 2000). Multiple functional groups on the activated carbon's surface are a sign of a favorable precondition for efficient adsorption.. Scanning Electron Micrograph for TSAAC was captured at 4000x magnification and presented in Figure 3. The morphology presented a fibrous, irregular surface with cavities of various sizes. This external structure characteristics observed may be as result of the chemical and thermal activation process.

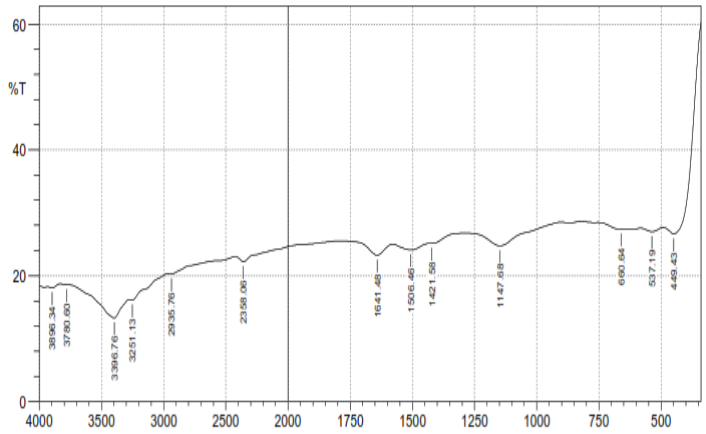


Fig 2: %Transmittance against wave numbers for TSAAC



Fig 3: SEM for TSAAC

3.2 Adsorption Kinetics

Figure 4 displays the influence of time on the percentage of EB dye adsorbed on TSAAC at various temperatures. It is observed that there is a significant raise in the % EB dye adsorbed as time increased from 0 to 50 minutes. A quasi-equilibrium trend was recorded when time was increased above 80 minutes. The initial high slope observed suggests initial rapid adsorptive uptake of the adsorbate. This occurrence could likely be described by the fact that all of the reaction sites were empty at the start of the sorption process, which led to a high degree of removal.

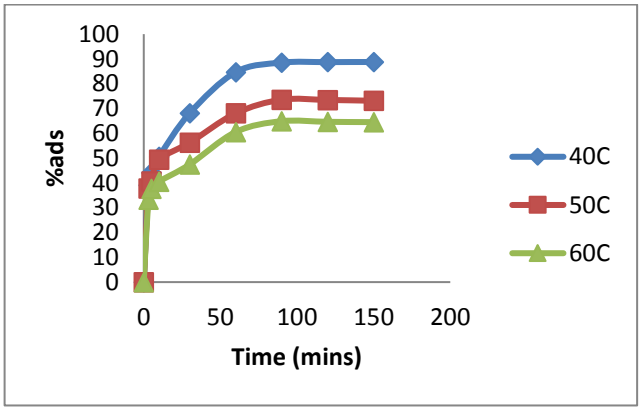


Fig. 4: Effect of time on %EB dye adsorbed at various temperatures

Analysis of kinetic data is very important in adsorption study. It gives an insight of the adsorptive uptake rate which aids the prediction of the mechanism of sorption and rate-controlling steps. To comprehend therefore, the adsorption kinetics of EB dye onto TSAAC at various temperatures, the PFO, PSO and Elovich kinetic models were investigated.

Figures 5, 6 and 7 are plots of PFO (equation 3), PSO (equation 4) and elovich (equation 5) models. The coefficient of determination displayed in figures 5 to 7 are found to be high for the models under investigation. The R^2 values were found to be generally > 0.911, > 0.974 and >0.997 for PFO, Elovich and PSO respectively. These findings show that the PSO kinetic model recorded the highest coefficient of determination, therefore, best described the adsorption system when compared with the Elovich and PFO models. The PSO model most describes the adsorption of species in solution. It is assumed for PSO adsorption kinetics that The interaction between the adsorbent and

adsorption sites on the adsorbent surface during the adsorption process affects the adsorption rate (Wang et al., 2022).

Figure 8 presents a graph of the intra-particle diffusion model that has been linearized. It can be seen that the plots in general track the same trend and did not go through the origin at the different temperatures under consideration. A difference in the rate of mass transfer at the beginning and end of the adsorptive process could be the cause of the observed departure from the point of origin. The plots' departure from the origin suggests that surface adsorption and intra-particle diffusion may both play a role in the rate-determining step, rather than just intra-particle diffusion determining the rate-limiting step. (Okoye et al., 2019).

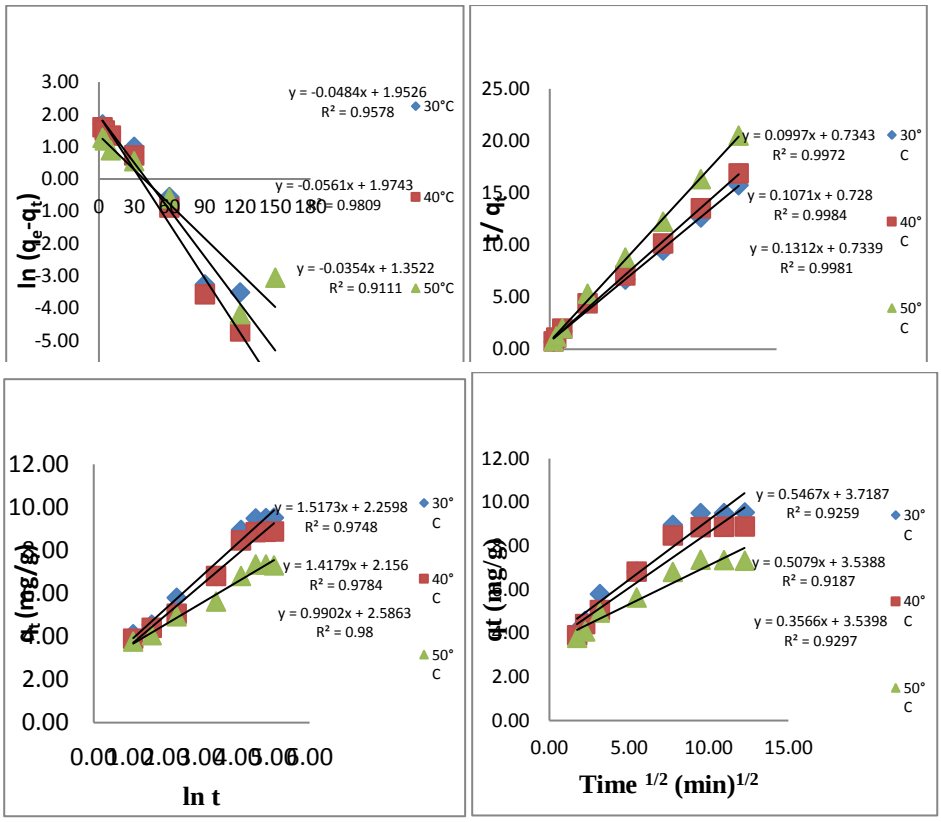


Fig 7: Elovich Plot for EB dye on TSAA

Fig 8: Intra-Particle Diffusion for EB dye on TSAA

Table 3 displays the calculated parameters from the slopes and intercepts of Figures 5 to 8 for Pseudo-first Order, Pseudo-second order, Elovich and Intra-particle Diffusion kinetic models

Table 3 : Calculated kinetic parameters for the adsorption of Erythrosin B on TSAA

Kinetic Model	Temperature (°C)		
	30	40	50
Pseudo first-order			
K_1 (min^{-1})	0.0484	0.0561	0.0354
q_e (mg/g)	7.047	7.2016	3.8659
R^2	0.9578	0.9809	0.9111
Pseudo second-order			
K_2 (g/mg min)	0.0135	0.0158	0.0235

q_e (mg/g)	10.0301	9.3371	7.622
R^2	0.9972	0.9984	0.9981
Elovich			
α (mg/g min)	6.7281	6.4866	13.4913
β (g/mg)	0.6591	0.7053	1.0099
R^2	0.9748	0.9784	0.98
Intraparticle diffusion			
K_d (g/mg $min^{1/2}$)	0.5467	0.5079	0.3566
δ	3.7187	3.5388	3.5398
R^2	0.9259	0.9187	0.9297

3.3 Statistical Analysis

3.3.1 One-way factorial analyses

The influence of temperature at predetermined times on the uptake of EB dye onto TSAAC is pictured in Figure 4. ANOVA was employed to establish if a statistical significance difference exists between the percentages of EB dye adsorbed on TSAAC at various time intervals. Table 4 depicts that the probability value is lower than 0.05 (critical value). This implies that the alternate hypothesis (there is significant difference between the EB dye's adsorptive performances on TSAAC at different time intervals) is accepted and null hypothesis (there is no significant difference between the EB dye's adsorptive performances on TSAAC at different time intervals) rejected. Furthermore, the significant F-Value presented in Table 4 shows that there are differences in the means but the exact places where the differences occurred was not revealed. To locate the spot where these differences occurred, the Tukey's HSD post hoc analysis was employed (Okoye et al., 2019).

Table 4: ANOVA Table for influence of time variation on %EB dye adsorbed onto TSAAC

ANOVA

Ads

	Sum of Squares	df	Mean Square	F	Sig.
Between Groups	5827.647	7	832.521	8.858	.000
Within Groups	1503.828	16	93.989		
Total	7331.475	23			

From Table 5, the recorded P-values for these sets: 3 and 5minutes, 10 minutes, 30 minutes; 5 and 3 minutes, 10 minutes, 30 minutes, 60 minutes; 10 and 3 minutes, 5 minutes, 30 minutes, 60 minutes; 30 and 3 minutes, 5 minutes, 10 minutes, 60 minutes, 90 minutes, 120 minutes, 150 minutes; 60 and 10 minutes, 30 minutes, 90 minutes, 120 minutes, 150 minutes; 90 and 30 minutes, 60 minutes, 120 minutes, 150 minutes; 120 and 30 minutes, 60 minutes, 90 minutes, 150 minutes; 150 and 30 minutes, 60 minutes, 90 minutes, 120 minutes are greater than 0.05 thus do not have statistical difference in the percentage of EB dye adsorbed. However, P-values for these times: 3 and 60 minutes, 90 minutes, 120 minutes and 150 minutes, 5 and 90 minutes, 120 minutes and 150 minutes; 10 and 90 minutes, 120 minutes and 150 minutes; 60 and 3 minutes, 5 minutes; 90 and 3 minutes, 5 minutes, 10 minutes; 120 and 3 minutes, 5 minutes, 10 minutes; 150 and 3 minutes, 5 minutes, 10 minutes are less than 0.05 therefore, there exist a statistical significant difference in their adsorptive uptake.

3.3.2 Post Hoc Tests

Table 5: Tukey's Honest Significant Difference post hoc tests analysis

Tukey HSD

(I) Time	(J) Time	Mean Difference (I-J)	Std. Error	Sig.	95% Confidence Interval	
					Lower Bound	Upper Bound
3	5	-4.10667	7.91578	.999	-31.5123	23.2989
	10	-10.13000	7.91578	.894	-37.5356	17.2756
	30	-20.58667	7.91578	.225	-47.9923	6.8189
	60	-34.40000*	7.91578	.009	-61.8056	-6.9944
	90	-38.95667*	7.91578	.003	-66.3623	-11.5511
	120	-38.89000*	7.91578	.003	-66.2956	-11.4844
	150	-38.76333*	7.91578	.003	-66.1689	-11.3577
5	3	4.10667	7.91578	.999	-23.2989	31.5123
	10	-6.02333	7.91578	.993	-33.4289	21.3823
	30	-16.48000	7.91578	.464	-43.8856	10.9256
	60	-30.29333*	7.91578	.025	-57.6989	-2.8877
	90	-34.85000*	7.91578	.008	-62.2556	-7.4444
	120	-34.78333*	7.91578	.008	-62.1889	-7.3777
	150	-34.65667*	7.91578	.009	-62.0623	-7.2511
10	3	10.13000	7.91578	.894	-17.2756	37.5356
	5	6.02333	7.91578	.993	-21.3823	33.4289
	30	-10.45667	7.91578	.878	-37.8623	16.9489
	60	-24.27000	7.91578	.103	-51.6756	3.1356
	90	-28.82667*	7.91578	.036	-56.2323	-1.4211
	120	-28.76000*	7.91578	.036	-56.1656	-1.3544
	150	-28.63333*	7.91578	.037	-56.0389	-1.2277
30	3	20.58667	7.91578	.225	-6.8189	47.9923
	5	16.48000	7.91578	.464	-10.9256	43.8856
	10	10.45667	7.91578	.878	-16.9489	37.8623
	60	-13.81333	7.91578	.661	-41.2189	13.5923
	90	-18.37000	7.91578	.340	-45.7756	9.0356
	120	-18.30333	7.91578	.344	-45.7089	9.1023
	150	-18.17667	7.91578	.352	-45.5823	9.2289
60	3	34.40000*	7.91578	.009	6.9944	61.8056
	5	30.29333*	7.91578	.025	2.8877	57.6989
	10	24.27000	7.91578	.103	-3.1356	51.6756
	30	13.81333	7.91578	.661	-13.5923	41.2189
	90	-4.55667	7.91578	.999	-31.9623	22.8489
	120	-4.49000	7.91578	.999	-31.8956	22.9156
	150	-4.36333	7.91578	.999	-31.7689	23.0423
90	3	38.95667*	7.91578	.003	11.5511	66.3623
	5	34.85000*	7.91578	.008	7.4444	62.2556
	10	28.82667*	7.91578	.036	1.4211	56.2323
	30	18.37000	7.91578	.340	-9.0356	45.7756
	60	4.55667	7.91578	.999	-22.8489	31.9623
	120	.06667	7.91578	1.000	-27.3389	27.4723
	150	.19333	7.91578	1.000	-27.2123	27.5989
120	3	38.89000*	7.91578	.003	11.4844	66.2956
	5	34.78333*	7.91578	.008	7.3777	62.1889
	10	28.76000*	7.91578	.036	1.3544	56.1656

	30	18.30333	7.91578	.344	-9.1023	45.7089
	60	4.49000	7.91578	.999	-22.9156	31.8956
	90	-.06667	7.91578	1.000	-27.4723	27.3389
	150	.12667	7.91578	1.000	-27.2789	27.5323
150	3	38.76333*	7.91578	.003	11.3577	66.1689
	5	34.65667*	7.91578	.009	7.2511	62.0623
	10	28.63333*	7.91578	.037	1.2277	56.0389
	30	18.17667	7.91578	.352	-9.2289	45.5823
	60	4.36333	7.91578	.999	-23.0423	31.7689
	90	-.19333	7.91578	1.000	-27.5989	27.2123
	120	-.12667	7.91578	1.000	-27.5323	27.2789

*. The mean difference is significant at the 0.05 level.

3.4 Experimental Design

A set of 30 experimental run derived from the Central Composite Design technique of the Response Surface Methodology was evaluated to ascertain the combined effect of the process variables (adsorbent dosage, time, temperature and pH) on the response variable (%EB dye uptake). To explain the relationship between the output and input variables, statistical model results were compared between the linear, two-factor interactions, quadratic, and cubic models. A low standard variation and high regression coefficient (R^2) were employed to decide the most suitable model for the adsorption process (Banza et al., 2023).

Table 6: Model Summary Statistics

Source	Std. Dev.	R-Squared	Adjusted R-Squared	Predicted R-Squared	PRESS	
Linear	7.80	0.7931	0.7599	0.7192	2065.25	
2FI	8.92	0.7944	0.6862	0.6758	2384.02	
Quadratic	0.87	0.9984	0.9970	0.9910	66.03	Suggested
Cubic	0.84	0.9993	0.9972	0.9033	711.48	Aliased

On Table 6, the quadratic model recorded the highest R^2 value of 0.9984, when measured with linear and 2FI models. Also, the quadratic model presented the least predicted error sum of squares (PRESS) value of 66.03 when measured with Linear model (2065.25), 2FI model (2384.02) and cubic model (711.48) thus an indication that the quadratic model best approximated the experimental data. Tthe Predicted R^2 and adjusted R^2 values of 0.9910 and 0.9970 are regarded as being in a reasonable agreement owing to the fact that the difference in their recorded values is less than 0.2. The recorded coefficient of determination (R^2) value of 0.9984 reveals that only about 0.16% of the total variations could not be explained by the model. Anchored on the adequacy test results, the quadratic model was selected for other computations.

Table 7: ANOVA for EB dye adsorption response surface quadratic model

Source	Sum of Squares	df	Mean Square	F-Value	p-value
Model	7342.475413	14	524.4625295	686.293614	< 0.0001
A-Dosage	24.04001667	1	24.04001667	31.4579383	< 0.0001
B-Time	422.3526	1	422.3526	552.676075	< 0.0001
C-Temp	323.4004167	1	323.4004167	423.190654	< 0.0001
D-pH	5062.253067	1	5062.253067	6624.29012	< 0.0001
AB	1.265625	1	1.265625	1.65615331	0.2176
AC	0.1156	1	0.1156	0.15127018	0.7028
AD	0.697225	1	0.697225	0.91236464	0.3546

BC	0.050625	1	0.050625	0.06624613	0.8004
BD	5.7121	1	5.7121	7.47465745	0.0154
CD	2.146225	1	2.146225	2.80847616	0.1145
A^2	32.04207619	1	32.04207619	41.929158	< 0.0001
B^2	56.35047619	1	56.35047619	73.7382935	< 0.0001
C^2	307.0519048	1	307.0519048	401.797554	< 0.0001
D^2	1344.320019	1	1344.320019	1759.1309	< 0.0001
Residual	11.46293333	15	0.764195556		
Lack of Fit	11.46293333	10	1.146293333		

Table 7 summarized the ANOVA result. From the presented data, the significance of the model and its terms were determined considering the P-value. A 95% level of confidence was used in the probability analysis. Terms with p-value ≥ 0.05 were considered insignificant while terms with p-value < 0.05 were taken to be significant. The magnitude of the relevance of the model and its terms was also evaluated with the Fisher's F-test values. Model F-value is determined by computing the ratio of mean square residual and mean square regression. F-value of 686.29 indicates that the model is significant. On Table 7, model terms: A-Dosage, B-Time, C-Temperature, D-pH, BD, A^2, B^2, C^2 and D^2 are seen to be statistically significant (p-value<0.05). Equation (10) displays the model that relates the response variable and independent variables (adsorbent dosage, contact time, temperature and pH):

$$\%Ads = 88.01 + 1.00A + 4.19B - 3.67C - 14.52D - 0.28\,AB - 0.085AC - 0.21AD + 0.056BC + 0.60BD + 0.37CD - 1.08A^2 - 1.43B^2 - 3.35C^2 - 7.00D^2 \quad (10)$$

Equation (11) was obtained after removing the insignificant model terms

$$\%Ads = 88.01 + 1.00A + 4.19B - 3.67C - 14.52D + 0.60BD - 1.08A^2 - 1.43B^2 - 3.35C^2 - 7.00D^2 \quad (11)$$

A graphical description of the model predictions over the range of experimental data within the design space was presented in Figure 9. For a high correlation, it is expected that the points Predicted vs. actual plot should scatter around the 45˚ line. This expected trend was followed on Figure 9 showing robust model prediction.

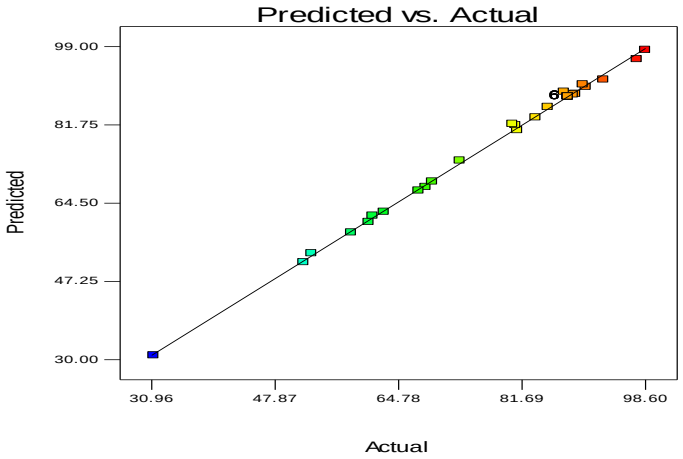


Fig. 9: RSM predicted vs actual for adsorption of EB dye

Table 8: Design of experimental matrix for Adsorption of EB dye on TSAAC

								Residuals	
S/N	Dosage	Time	Temp.	pH	% Ads	RSM	ANFIS	RSM	ANFIS
1	1	90	50	6	80.83	81.685	80.83	-0.855	0
2	3	90	50	6	87.64	88.01	88.01	-0.37	-0.37
3	5	90	50	6	85.26	85.69	85.26	-0.43	0
4	2	120	60	8	61.26	61.74	61.26	-0.48	0
5	3	90	50	6	88.72	88.45	88.01	0.27	0.71
6	4	120	60	4	90.48	90.13	90.48	0.35	0
7	3	150	50	6	90.06	90.67	90.06	-0.61	0
8	4	120	40	4	98.6	98.26	98.6	0.34	0
9	3	90	50	6	87.88	88.01	88.01	-0.13	-0.13
10	2	60	60	8	51.79	51.48	51.79	0.31	0
11	4	60	40	8	60.72	60.35	60.72	0.37	0
12	4	120	40	8	69.41	69.26	69.41	0.15	0
13	2	120	40	4	97.46	96.24	97.46	1.22	0
14	2	120	40	8	68.52	68.07	68.52	0.45	0
15	4	60	60	8	52.88	53.46	52.88	-0.58	0
16	4	60	60	4	83.58	83.39	83.58	0.19	0
17	4	60	40	4	92.87	91.74	92.87	1.13	0
18	3	90	50	6	88.24	88.01	88.01	0.23	0.23
19	3	90	30	6	80.42	81.97	80.42	-1.547	0
20	2	120	60	4	88.72	88.01	88.72	0.71	0
21	2	60	60	4	81.07	80.56	81.07	0.51	0
22	3	90	50	10	31.25	30.96	31.25	0.29	0
23	3	90	50	6	88.57	88.01	88.01	0.56	0.56
24	2	60	40	4	89.03	88.59	89.03	0.44	0
25	4	120	60	8	62.8	62.6	62.8	0.2	0
26	2	60	40	8	58.33	58.04	58.33	0.29	0
27	3	90	50	2	87.48	89.05	87.48	-1.57	0
28	3	90	50	6	87.03	88.01	88.01	-0.98	-0.98
29	3	30	50	6	73.21	73.89	73.21	-0.68	0
30	3	90	70	6	67.55	67.29	67.55	0.26	0

3.5 ANFIS

The adaptive neuro-fuzzy inference system (ANFIS) employed a hybrid learning algorithm that uses the least square and gradient method to model the behaviour of the adsorptive uptake of EB dye on TSAAC. The Sugeno fuzzy logic designer structure was illustrated in Figure 10. FIS was generated by assigning two membership functions (MFs) to each element in the input layer. The ANFIS architecture is given on Table 9

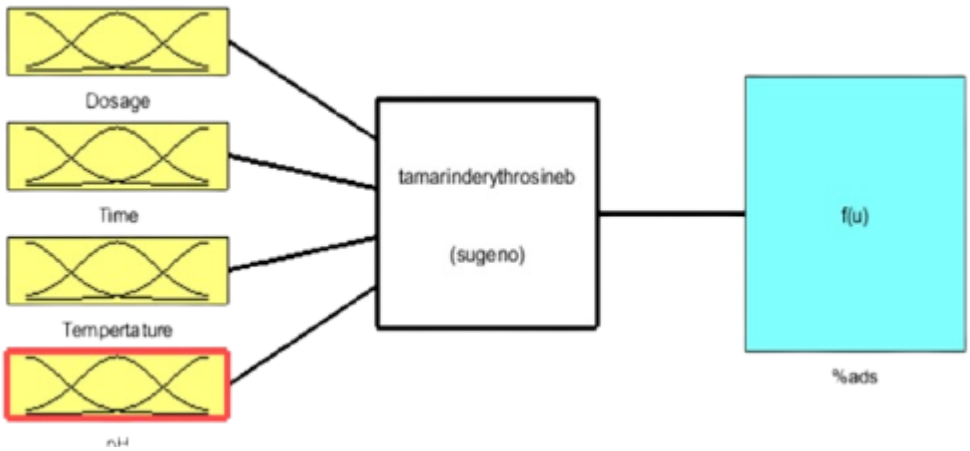


Fig. 10: Anfis Fuzzy Logic Analyzer

Table 9: ANFIS architecture network specifications

Characterizations	Optimum method	FIS	Number of nodes	Number of linear parameters	Number of nonlinear parameters	Total number of parameters	Number of fuzzy rules
Type/Value	Hybrid	Grid partition	55	80	24	104	16

The ANFIS 30-dataset was trained at 30 epoch iterations with error tolerance of zero. The ANFIS modeling was completed with training error of 0.25721. The ANFIS predicted percentage of EB dye removed was presented in Table 8. A coefficient of determination very close to unity (0.999) obtained in the ANFIS modeling affirms its robust capability in predicting the adsorption of EB dye using TSAAC. The primary benefit of ANFIS is that it lowers error by adding self-learning capabilities to fuzzy controllers. (Arora and Keshari, 2021). Figure 11 shows an example of a fuzzy logic controller using Ruleviewer. The fuzzy inference procedure during the simulation is displayed in the ruleviewer block. Using fuzzy logic to create a mapping from a given input to an output is known as fuzzy inference. Figure 11 shows the four inputs of adsorptive uptake of EB dye onto TSAAC matrix: input 1(dosage), input2(time), input 3 (temperature), input 4 (pH) and output (% EB dye adsorbed). Sampling run 23 of the matrix (Table 8) at 3g adsorbent dosage, 90 mins contact time, 50˚C solution temperature and pH of 6, a prediction of 88% was recorded.

3.6 Three dimensional surface plots for adsorptive uptake of Erythrosine B dye on TSAAC

The interactive effect of temperature and adsorbent dosage for the adsorptive uptake of EB dye with TSAAC was displayed in Figure 12. The independent variables' simultaneous rise (temperature and adsorbent dosage) within the design space was synergetic on the dependent variable (% EB dye adsorbed). The rise in kinetic energy, which lowers the viscosity of the solution and increases the mobility of the erythrosine B dye molecules on the adsorbent surfaces, may be the reason behind the observed rise in the percentage of EB dye removal as the temperature is raised (Obayomi et al., 2024). The observed trend for adsorbent dosage may be due to increased surface area as dosage increases. Above adsorbent dosage of 3g, the major effect observed on the dependent variable started to diminish. The latter trend, according to Zhao et al. (2023), was caused by the agglomeration of adsorbents; as adsorbent dosage increased further, the total adsorbent surface area and the availability of active surface sites decreased; a review beyond a temperature of 40˚C, there was a sharp decrease in the corresponding dependent variable. Figure 13 shows the illustration of the combined effects of time and adsorbent dosage on the response for the adsorption of erythrosine B onto TSAAC. It was noted that simultaneous rise in adsorbent dosage and contact time had a synergetic influence on the response variable.

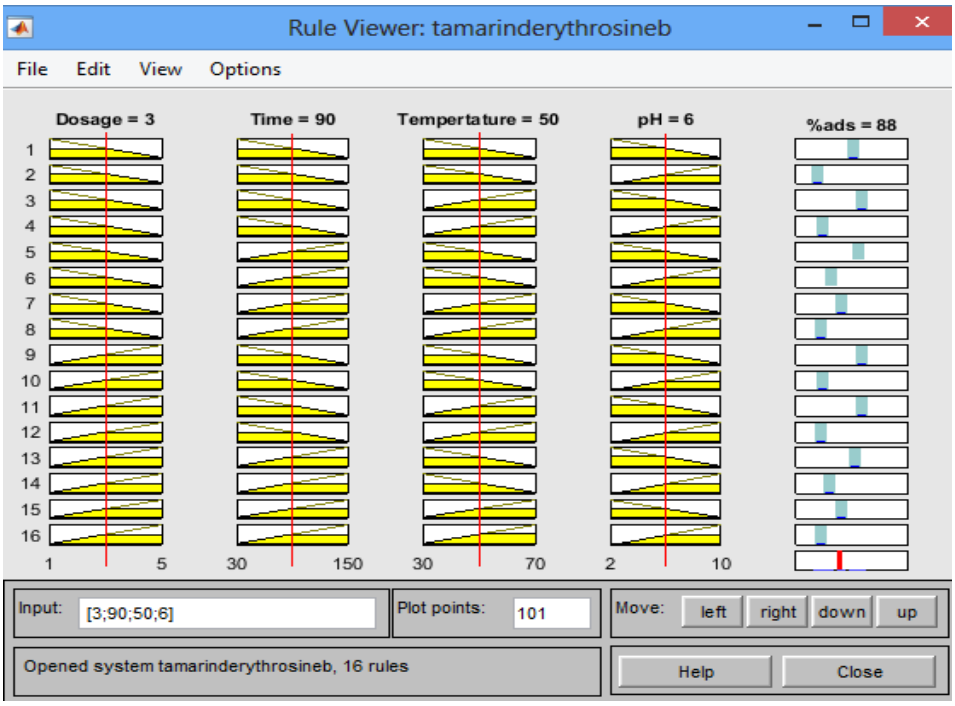


Fig. 11: Fuzzy logic controller with ruleviewer

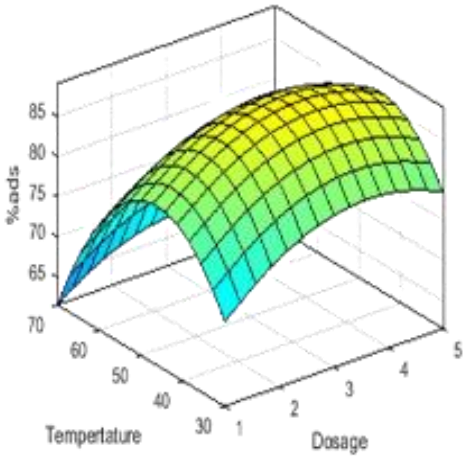


Fig. 12: 3D Surface plot for combined effect of temp. and dosage on the percentage of EB dye adsorbed.

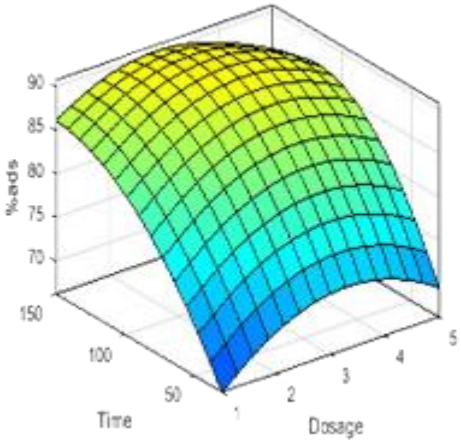


Fig. 13: 3D Surface plot for combined effect of time and dosage on the percentage of EB dye adsorbed.

Figure 14 diagrammatically illustrates the influence of pH and adsorbent dosage on the % EB dye adsorbed onto TSAAC with other variables held at their midpoints. As pH values were reviewed upwards, it was observed that there was an antagonistic effect on the response variable irrespective of the adsorbent dosage value investigated within the design space. The trend observed for in pH may be due to the fact that EB dye is an anionic dye. The curved architecture (canopy) observed in Figures 12, 13 and 14 implies that there are statistically significant quadratic terms in the model.

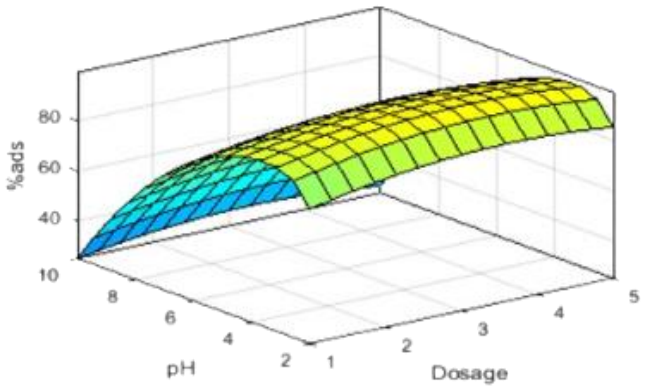


Fig. 14: 3D Surface plot for combined effect of pH and dosage on the % EB dye adsorbed.

3.7 Comparison of RSM and ANFIS Models

The suitability of the ANFIS and RSM models in approximating the experimental data for the adsorption of EB dye onto TSAAC was evaluated using the coefficient of determination (R^2), Hybrid fractional error function (HYBRID), Marquadt's Percent Standard Deviation (MPSD), and Average Relative Error (ARE). From Figures 15 and 16, both RSM and ANFIS models presented very high R^2 of 0.999 and 0.998 respectively. To further investigate the capability of the models in capturing the experimental data, error functions were employed. The lower the value of the error function for a model, the higher the predictive capability of the model. It is observed from Table10 that ANFIS consistently presented values lower than RSM for MPSD, HYBRID and ARE. Based on these findings, it can be stated that ANFIS outperformed RSM in predicting the experimental data.

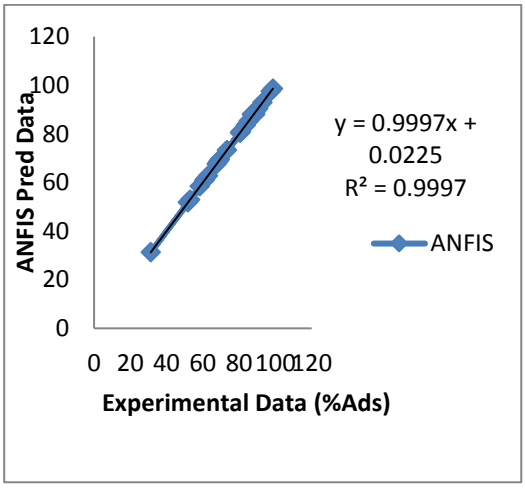


Fig. 15: A graph of ANFIS pred vs Exp. data

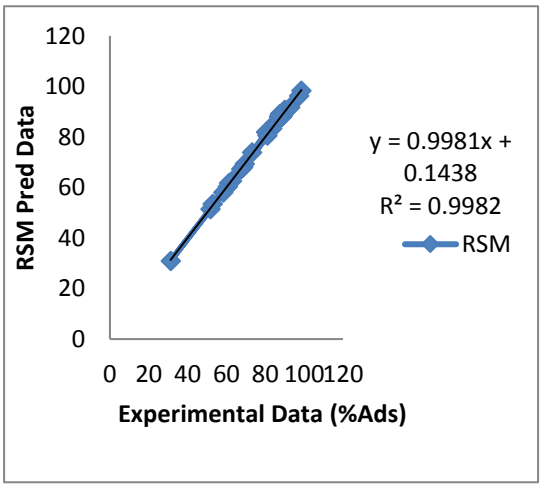


Fig. 16: A graph of RSM pred vs Exp. data

Table 10: Error function

Error Function	RSM	ANFIS
MPSD	0.892	0.315
HYBRID	0.008	0.001
ARE	0.007	0.001

3.8 Optimization

The optimization of the adsorptive uptake of EB dye on TSAAC was done using the genetic algorithm (GA). The GA optimization method predicted an optimal percentage of 96.73% EB dye adsorbed at 2.13g adsorbent dosage, 118 minutes contact time, 41˚C temperature and 4.2 solution pH experimental condition (Figure 17). To validate the optimization result, experiment at the GA determined condition was conducted. The experimentally obtained response value of 96.08% under the same process variable conditions closely matches the GA predicted value.

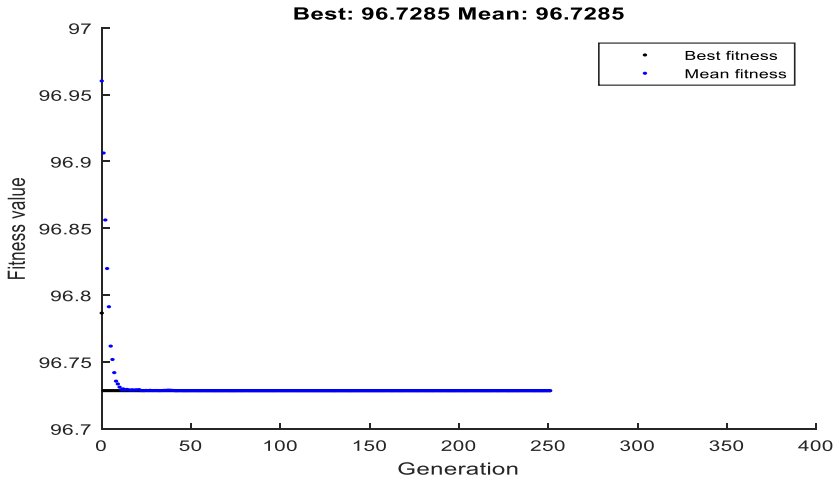


Fig. 17: GA Optimization fitness plot

4.0 Conclusion

The capability of tamarind seed, an agrowaste of regenerative resource to serve as adsorbent for the uptake of EB dye from waste water has been studied. This is in line with SDG Goal 6: secure access to water and sanitation. This research compared the predictive potential of ANFIS and RSM in modeling the adsorptive performance of TSAAC in the remediation of EB dye wastewater. The % EB dye adsorbed onto TSAAC was influenced by the independent variables such as adsorbent dosage, contact time, temperature and pH. The PSO model best described the adsorption kinetics of the system. ANOVA result revealed that there is significant difference at various time intervals among the adsorptive performances of EB dye on TSAAC. Findings from the error function computations revealed that ANFIS has higher capability in predicting the adsorption system. An optimal response value of 96.73% was recorded using genetic optimization. This study has shown that TSAAC can serve as an adsorbent for removal of EB dye from wastewater.

5.0 References

Abisha, B. R., Anish, C. I., Beautlin, N. R., Daniel, S. N. and Jaya, R. M. 2022 Adsorption and equilibrium studies of methyl orange on tamarind shell activated carbon and their characterization, Phosphorus, Sulfur, and Silicon and the Related Elements, 197(3), 225-230, 10.1080/10426507.2021.1993849.

Akpomie, K. G. and Conradie, J. 2020. Advances in application of cotton-based adsorbents for heavy metals trapping, surface modifications and future perspectives. Ecotoxicology and Environmental Safety,201 (110825),https://doi.org/10.1016/j.ecoenv.2020.110825.

Alabbad, E. A. 2020 Efficient removal of methyl orange from wastewater by polymeric chitosaniso-vanillin. Open Chem J. 7,16–25.

Alardhi, S. M., Fiyadh, S. S., Salman, A. D. and Adelikhah, M. 2023. Prediction of methyl orange dye (MO) adsorption using activated carbon with an artificial neural network optimization modelling. Heliyon, 9 (e12888), https://doi.org/10.1016/j.heliyon.2023.e12888.

Arora, S., Keshari, A. K. 2021. ANFIS–ARIMA modelling for scheming re-aeration of hydrologically altered rivers. J. Hydrol. 601, 126635, https://doi.org/10.1016/j.jhydrol.2021.126635.

Banza, M., Seodigeng, T. and Rutto, H. 2023. Comparison Study of ANFIS, ANN, and RSM and Mechanistic Modeling for Chromium(VI) Removal Using Modified Cellulose Nanocrystals–Sodium Alginate (CNC–

Alg). Arabian Journal for Science and Engineering. 48, 16067–16085. https://doi.org/10.1007/s13369-023-07968-6.

Coates, J. 2000. Interpretation of Infrared spectra, a practival approach. Encyclopedia of analytical chemistry. Chichester: John Wiley & Sons.

Benjelloun, M., Miyah, Y., Evrendilek, G. A., Zerrouq, F. and Lairini, S. 2021. Recent Advances in Adsorption Kinetic Models: Their Application to Dye Types. Arabian Journal of Chemistry, 14(103031), https://doi.org/10.1016/j.arabjc.2021.103031 1878-5352.

Elfadil, D., Pelle, F. D., Compagnone, D. and Amine, A. 2022. Green Synthesis of Molecularly Imprinted Polymers for Dispersive Magnetic Solid-Phase Extraction of Erythrosine B Associated with Smartphone Detection in Food Samples. *Materials*, *15*(21), 7653, https://doi.org/10.3390/ma15217653.

Fito, J., Abewaa, M., Mengistu, A., Angassa, K., Ambaye, A. D., Moyo, W. and Nkambule, T. 2023. Adsorption of methylene blue from textile industrial wastewater using activated carbon developed from Rumexabyssinicus plant. Scientific report, 13(5427). https://doi.org/10.1038/s41598-023-32341-w.

Garcia, V.S.G., de Freitas Tallarico, L., Rosa, J. M., Suzuki, C. F., Roubicek, D. A., Nakano, E. and Borrely, S. I. 2021. Multiple adverse effects of textile effluents and reactive Red 239 dye to aquatic organisms. Environ. Sci. Pollut. Res. 28, 63202–63214.

Hambisa, A. A., Regasa, M. B., Ejigu, H. G. and Senbeto, C. B. 2023. Adsorption studies of methyl orange dye removal from aqueous solution using Anchote peel-based agricultural waste adsorbent. Applied Water Science,13(24), 1-11. https://doi.org/10.1007/s13201-022-01832-y.

Hung, D. Q., Dinh, L. X., Tung, N. V., Huong, L. M., Lien, N. T., Minh, P. T. and Le, T. 2023. The adsorption kinetic and isotherm studies of metal ions (Co2+, Sr2+, Cs+) on Fe3O4 nanoparticle of radioactive importance. Results in Chemistry. 6 (101095). https://doi.org/10.1016/j.rechem.2023.101095.

Janani, V. A., Gokul, D., Dhivya, N., Nesarani, A., Mukilan, K., Kumar, A. S. Kumar, M. V. 2023. Optimization Studies on Methyl Orange (MO) Dye Adsorption using Activated Carbon Nanoadsorbent of Ocimumbasilicum Linn Leaves. Hindawi Journal of Nanomaterials, 7969512, 1-14. https://doi.org/10.1155/2023/7969512.

Nascimento, R.S., Corrêa, J.A.M., Figueira, B.A.M., Pinheiro, P.A., Silva, J.H., Freire, P.T.C. and Quaranta, S. 2022.From mining waste to environmetal remediation: a nanoadsorbent from Amazon bauxite tailings for the removal of erythrosine B dye. Applied Clay Science222, 106482, https://doi.org/10.1016/j.clay.2022.106482

Nure, J. F., Mengistu, A., Abewaa, M., Angassa, K., Moyo, W., Phiri, Z., Mafa, P. J., Kuvarega, A. T. and Nkambule, T. T. I. 2023. Adsorption of Black MNN reactive dye from tannery wastewater using activated carbon of RumexAbysinicus. Journal of the Taiwan Institute of Chemical Engineers. 151 (105138), https://doi.org/10.1016/j.jtice.2023.105138.

Obayomi, K. S., Lau, S. Y., Danquah, M. K., Zhang, J., Chiong, T., Obayomi, O. V., Meunier, L. and Rahman, M. M. 2024. A response surface methodology approach for the removal of methylene blue dye from wastewater using sustainable and cost-effective adsorbent. Process safety and environmental protection, 184, 129-150, https://doi.org/10.1016/j.psep.2024.01.106.

Okoye, C. C., Onukwuli, O. D., Okey-Onyesolu, C. F. 2019. Utilization of salt activated Raphia hookeri seeds as biosorbent for Erythrosine B dye removal: Kinetics and thermodynamics studies. Journal of King Saud University – Science, 31, 849-858, https://doi.org/10.1016/j.jksus.2017.11.004.

Phothitontimongkol, T and Prasertboonya, K. 2024. A fast removal of methyl orange from an aquatic system utilizing activated carbon from waste tamarind wood. Desalination and Water Treatment. 317(100267), 1-9.

Pipíška, M., Krajˇcíková, E.K., Hvostik, M., Frišták, V., Duriška, L., ˇ Cerniˇcková, I., Ka ˇnuchová, M., ˇ Conte, P. and Soja, G. 2022. Biochar from Wood Chips and Corn Cobs for Adsorption of Thioflavin T and Erythrosine B. Materials, 15, 1492. https:// doi.org/10.3390/ma15041492.

Revellame, E. D., Fortela, D. L., Sharp, W., Hernandez, R. and Zappi, M. E. 2020. Adsorption kinetic modeling using pseudo-first order and pseudo-second order rate laws: A review. Cleaner Engineering and Technology, 1(100032). https://doi.org/10.1016/j.clet.2020.100032.

Serban, G.V., Iancu, V.I., Dinu, C., Tenea, A., Vasilache, N., Cristea, I., Niculescu, M., Ionescu, I. and Chiriac, F.L. 2023. Removal Efficiency and Adsorption Kinetics of Methyl Orange from Wastewater by Commercial Activated Carbon. Sustainability, 151(2939), https://doi.org/10.3390/ su151712939.

Sulthana, R., Taqui, S. N., Syed, U. S., Khan, T. M. Y., Khadar, S. D. A., Mokashi, I., Shahapurkar, K., Kalam, M. A., Murthy, H. C. A. and Syed, A. A. 2022. Adsorption of Crystal Violet Dye from Aqueous Solution using

Industrial Pepper Seed Spent: Equilibrium, Thermodynamic, and Kinetic Studies. Hindawi Adsorption Science & Technology, 9009214, 1 - 20. https://doi.org/10.1155/2022/9009214

Surela, A. K., Chhachhia, L. K.Surela, V. K. and Meena, P. L. 2024. Polypyrrole-Based composites for dyes removal from contaminated water. Reference module in materials science and materials engineering. https://doi.org/10.1016/B978-0-323-95486-0.00019-3.

Tomar, T., Kahandawala, N., Kaur, J., Thounaojam, L., Choudhary, I. and Bera, S. 2023. Bioremediation of synthetic dyes from wastewater by using microbial nanocomposites: An emerging field for water pollution management. Biocatal. Agric. Biotechnol., 51, 102767.

Wang, J. and Guo, X. 2023. Adsorption kinetics and isotherm models of heavy metals by various adsorbents: An overview. Critical Reviews in Environmental Science and Technology, DOI: 10.1080/10643389.2023.2221157

Wang, M., Janssen, ABG., Bazin, J., Strokal, M., Ma, L. and Kroeze, C. 2022. Accounting for interactions between sustainable development goals is essential for water pollution control in China. Nat Commun,13:1–13. https://doi.org/10.1038/s41467- 022-28351-3.

Wang, T., Jiang, M., Yu, X., Niu, N. and Chen, L. 2022. Application of lignin adsorbent in wastewater treatment: A review. Separation and purification technology, 302(122116), https://doi.org/10.1016/j.seppur.2022.122116.

Wu. L., Liu, X., Lv, G., Zhu, R., Tian, L., Liu, M., Li, Y., Rao, W., Liu, T. and Liao, L. 2021. Study on the adsorption properties of methyl orange by natural one-dimensional nano-mineral materials with diferent structures. Sci Rep. 11(10640).

Yaqub, A., Misbah, S., Ajab, H., Zia, M. &Haq, U. 2023. Activated carbon derived from Dodonaeaviscosa into beads of calcium-alginate for the sorption of methylene blue (MB): Kinetics, equilibrium and thermodynamics. J. Environ. Manag. 327, 116925.

Zayed, A. M., Metwally, B. S., Masoud, M. A., Mubarak, M. F., Shendy, H., Abdelsatar, M. M., Petrounias, P., Ragab, A. H., Hassane, A. A. and Abdel Wahed, M. S. M. 2023.Efficient dye removal from industrial wastewater using sustainable activated carbon and its polyamide nanocomposite derived from agricultural and industrial wastes in column systems. RSC Adv., 13, 24887–24898.

Zhao, W., Hao, C., Guo, Y., Shao, W., Tian, Y. and Zhao, P. 2023. Optimization of Adsorption Conditions Using Response Surface Methodology for Tetracycline Removal by MnFe2O4/Multi-Wall Carbon Nanotubes. Water, 15, 2392. https://doi.org/10.3390/ w15132392